Relationship between extinction magnitude and climate change during major marine/terrestrial animal crises

Kunio Kaiho

Department of Earth Science, Tohoku University, Aoba-aza, Aramaki, Aoba-ku, Sendai 980-8578, Japan

5 *Correspondence to*: Kunio Kaiho (kunio.kaiho.a6@tohoku.ac.jp)

Abstract. Major mass extinctions in the Phanerozoic Eon occurred during abrupt global climate changes accompanied by environmental destruction driven by large volcanic eruptions and projectile impacts. Relationships between land temperature anomalies and terrestrial animal extinctions as well as the difference in response between marine and terrestrial animals to abrupt climate changes in the Phanerozoic have not been quantitatively evaluated. My analyses show that the magnitude of

10 major extinctions in marine invertebrates and that of terrestrial tetrapods correlate well with the coincidental anomaly of global and habitat surface temperatures during biotic crises, respectively, regardless of the difference between warming and cooling (correlation coefficient $R = 0.92$–0.95). More than 35 % of marine genera and 60 % of marine species loss correlate to > 7 °C global cooling and > 9 °C global warming. Marine animals are more likely than tetrapods to become extinct under a habitat temperature anomaly, possibly due to a higher sensitivity of marine animals to temperature change than terrestrial

15 animals, which have access to places of refuge. These relationships indicate that abrupt changes in climate and environment associated with high energy input by volcanism and impact relate to the magnitude of mass extinctions.

1 Introduction

There are two habitat realms for animals: marine and terrestrial realms. Major mass extinctions of animals have occurred

20 five times: 444, 372, 252, 201, and 66 million years ago (Ma) after fundamental animal diversification was finished at ~520 Ma, commonly marked by high extinction percentages of animals inhabiting the marine realm (Sepkoski, 1996; Bambach, 2006; Stanley, 2016; Fan et al., 2020); these events were driven by large volcanic eruptions and projectile impacts (Schulte et al., 2010; Davies et al., 2017; Burgess et al., 2017; Bond and Grasby, 2020; Kaiho et al., 2021a, 2021b, 2022). The last three mass extinctions after the initial diversification of tetrapods at ~300 Ma had high extinction percentages for terrestrial

25 tetrapods (Sahney et al., 2010) and marine animals (Sepkoski, 1996; Bambach, 2006; Stanley, 2016; Fan et al., 2020). These major biotic crises were related to abrupt global climate changes (Balter et al., 2008; Korte et al., 2009; Finnegan et al., 2011; Chen et al., 2011; Vellekoop et al., 2014; Chen et al., 2016) and the accompanying environmental changes, such as acid rain, ozone depletion, reduced sunlight and oceanic anoxia, driven by large volcanic eruptions and projectile impacts (Schulte et al., 2010; Bond and Grasby, 2020), and the relationship has not been quantitatively studied. Long-term surface

30 temperature changes did not cause mass extinctions because animals migrate to survive (McPherson et al., 2022). Abrupt

high energy input by volcanism and impact to the surface of the Earth caused abrupt climate changes accompanied by abrupt environmental destruction, leading to animal crises.

Recently, Song et al. (2021) showed that a good relationship ($R = 0.63$) between temperature change and marine extinction magnitude during the past 450 million years. I aimed to clarify the relationship between the magnitude of biotic crises in marine invertebrates and terrestrial vertebrates (tetrapods) and the global and habitat [marine or terrestrial realm] surface temperature anomalies during the five major mass extinctions as well as the late Guadalupian crisis, which was added to the list of major mass extinctions in some literature (Stanley and Yang, 1994; Rampino and Shen, 2019). The other minor crises are omitted because they remain to be studied in detail, especially the coincidence between biotic crises and climate changes.

2 Data and methods

2.1 Diversity reduction percentage

Although Song et al. (2021) analyzed extinction data compared to sea surface temperature (SST) changes, there is no confirmation of the exact coincidence between extinction rate and temperature change for minor extinctions. I used only data showing the coincidence of shallow marine extinctions and temperature changes from the same outcrop of sedimentary rocks for a more accurate result. Therefore, I analyzed the six mass extinctions and the modern extinction, which coincided with global climate changes. For the five major mass extinctions, I used three marine genera loss percentage data sets based on three different methods (well-preserved genera data of Sepkosky, 1996; Bambach, 2006; Stanley, 2016). They show that the largest loss percentage occurred at the end of the Permian (58–66%), the smallest loss at the Frasnian–Famennian boundary (F–F; 18–41%), and intermediate loss percentage at the other three mass extinctions (39–52 %) (Fig. 1a). The error for genera and species loss percentages is approximately ± 5 % for >15 % loss values (Stanley, 2016). I do not use their data for the end of the Guadalupian because the uncertain high loss % likely due to "smear back" (Signor-Lipps Effect) from the great end-Permian event is enhanced by the loss of record from lower sea level in the later Permian (Bambach, 2006) (Fig. 1a, Table 1). Instead, I use the marine species and genera diversity data of Fan et al. (data from China; Fan et al., 2020) for the end of the Guadalupian, which seems to be the most believable data because their sedimentary rock sequences of the GSSP section and nearby sections contain continuous sedimentary rocks without a time gap (Fan et al., 2020; Huang et al., 2019). The data from China are likely not affected by the Signor-Lipps Effect. I also used data of % extinction of Barnosky et al. (2011) and Ceballos et al. (2015) for the Holocene–Anthropocene marine and terrestrial species.

I calculated % extinction using the marine animal diversity data of Fan et al. (2020) for the end-Guadalupian extinction and terrestrial tetrapod diversity data of Benton (2013) and Sahney and Benton (2017) for the last four crises since the early diversification of terrestrial tetrapods in the Carboniferous. The genera (species) loss % is calculated using the formula of total number of extinction genera (species) for a mass extinction interval / total number of genera (species) in a substage just before the extinction (conventional method in Stanley [2016]). My calculation results are comparable with the genera extinction % data in substages of Bambach and likely Sepkosky due to the usage of similar methods. Whereas, the Stanley

65 method considered background extinction, which differs from my calculations (e.g. low extinction % for F–F of Stanley is due to the consideration of the high background extinction % [Fig. 1a]).

Tetrapod genera loss of Benton (2013) and Sahney and Benton (2017) are used to represent reduction percentage for terrestrial animals because it is difficult to obtain good data for diversity losses among insects and plants. The tetrapod species data were converted from genus extinction percentage to species extinction percentage using the relationship curve

70 between family and genera for tetrapods in Fig. 1c since the actual marine family/genus data mostly fit the conversion relationship curve of genus/species of Stanley (2016) (Figs. 1b, c).
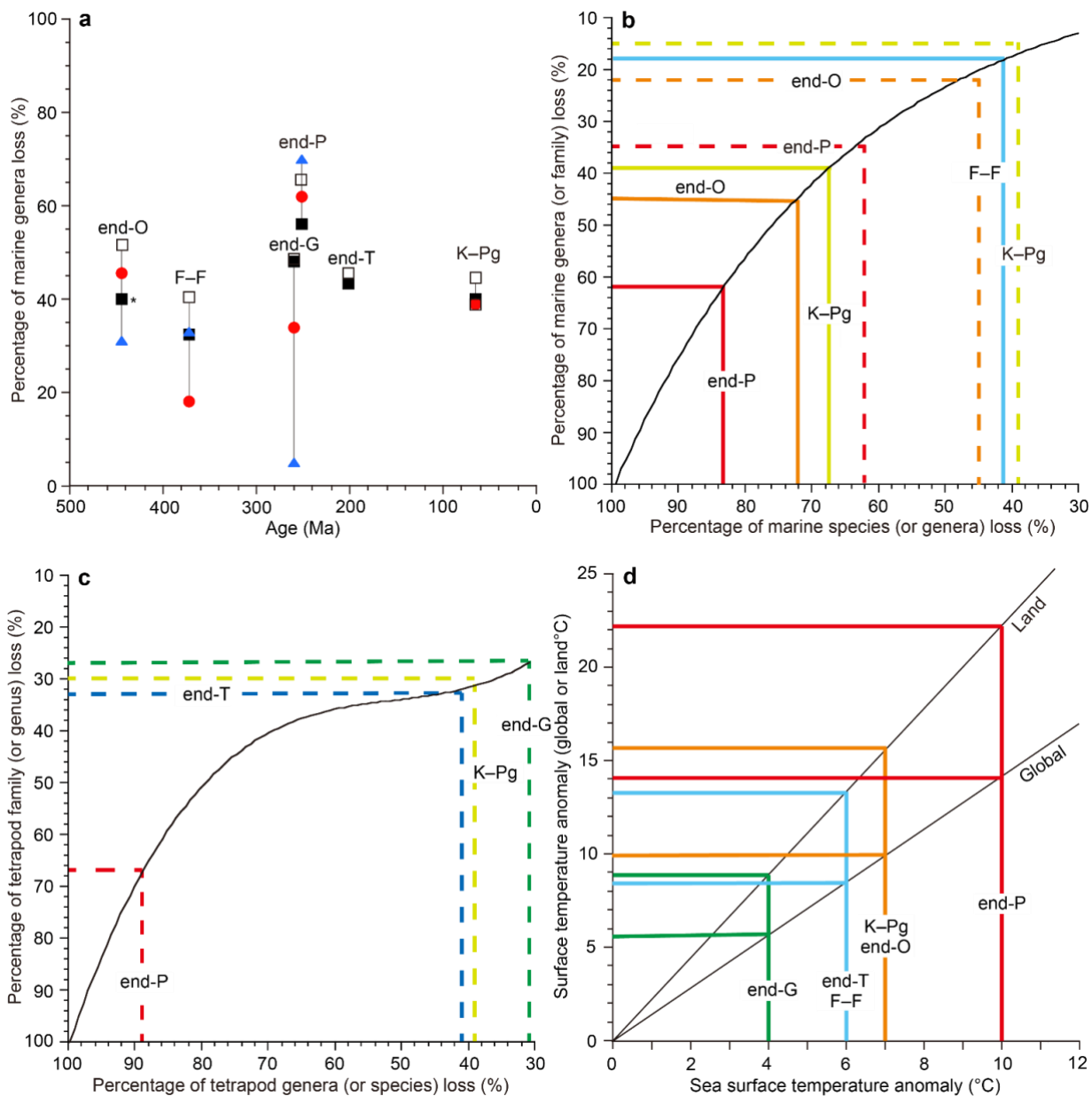

3

Figure 1: Marine genus loss (%) distribution (**a**), relationship between extinction percentages of species, genera, and families (**b** for marine invertebrates, **c** for terrestrial tetrapods) and between global surface temperature anomalies, land-surface temperature anomalies, and sea-surface temperature (SST) anomalies (**d**). Open square data from Sepkoski (1996), black square data from Bambach (2006), red circle data from Stanley (2016), and blue triangle data from Fan et al. (2020) in the graph (**a**). Graphs (**b**, **c**) were used to convert extinction percentages among species, genera, and families. Dashed lines show the genus-family loss relationship (**b**, **c**). The black curve in (**b**) is after Stanley (2016). Graph (**d**) is based on the model calculation data from Kaiho and Oshima (2017) and is used to convert between the global surface temperature anomaly, land-surface temperature anomaly (global mean), and SST anomaly (global mean). All data are from Table 1. O: Ordovician. F–F: Frasnian–Famennian boundary. P: Permian. T: Triassic. K–Pg: Cretaceous–Paleogene boundary. *Largest extinction % in the Late Ordovician mass extinction (LOME).

Table 1: Marine animal and tetrapod family and genus extinction percentages and global, sea, and land-surface temperature anomalies

Crisis	Age (Ma)	Marine family Ext (%)	Marine genus Ext (%)	Marine genus Ext (%)	Marine genus Ext (%)	Marine genus Ext (%)	Tetrapod family Ext (%)	Tetrapod Genus Ext (%)	Temp. anomaly (Global °C)	Temp. anomaly (SST °C)	Temp. anomaly (Land °C)
H–A	0	-				0*	-	*0.6*	*1*	*0.7*	*1.5*
K–Pg	66	15	**45**	**40**	39		30	**39***	*-10*	*-7*	*-16*
End-T	201.4	13	**46**	**43**			33	**41**	*-8*	*-6*	*-13*
End-P	251.9	35	**66**	**56**	62	70	67	**89**	*14*	*10*	*22*
End-G	259.8	-	48	48	34	5**	27	31	*6*	*4*	*9*
F–F	372	-	**41**	**35**	18	33	-	-	*-7*	*-5*	*-11*
End-O	445–444	22*	**52**	**40**	45.5	31	-	-	*10*	*7*	*16*
Reference		1, 2, 3*	1	4	5	6, 8*	9	10, 11*	13, 14	15–20	

Ext (%): extinction percentage. Data marked by bold letters are used in Figure 3. Italic letters show values converted using Figure 1b–d. O: Ordovician. F–F: Frasnian–Famennian boundary. G: Guadalupian. P: Permian. T: Triassic. K–Pg: Cretaceous–Paleogene boundary. *: corresponds to a reference marked by *. **: data without brachiopods because their diversity increased spanning the G–L boundary. **39*** at K–Pg is calculated from the data. References: 1: Sepkoski (1996); 2: Rampino et al. (2020); 3: Sepkoski (1982); 4: Bambach (2006); 5: Stanley (2016); 6: Fan et al. (2020); 7: Barnosky et al. (2011); 8: Ceballos et al. (2015); 9: Sahney et al. (2010); 10: Benton et al. (2013); 11: Sahney and Benton (2017); 12: IUCN (2021); 13: Waters et al. (2016); 14: Working Group I Contribution to the Fifth Assessment Report of the Intergovernmental Panel on Climate Change (2013); 15: Vellekoop et al. (2014); 16: Korte et al. (2009); 17: Chen et al. (2016); 18: Chen et al. (2011); 19: Balter et al. (2008); 20: Finnegan et al. (2011). Italic values are converted using Figs. 1b and 1d.

2.2 Surface temperature anomaly

The largest absolute sea-surface temperature (SST) anomalies during each crisis were obtained from the oxygen isotope ratios ($^{18}O/^{16}O$) of marine animal fossils (Balter et al., 2008; Korte et al., 2009; Finnegan et al., 2011, Chen et al., 2011) and the organic biomarker index (TEX_{86}) (Vellekoop et al., 2014) (Table 1). All the SST data are from low latitudes (Table 2). Global surface temperature anomalies at low latitudes are always intermediate values (near average values) regardless of (i) source latitudes of greenhouse gases or aerosols blocking sunlight (Kaiho and Oshima, 2017) (Table 1) and (ii) global warming and cooling because the highest anomaly appears at middle–high latitudes in the source hemisphere and the lowest anomaly appears at middle–high latitudes in the other hemisphere based on warming case data (Pinsky et al., 2019) and cooling case data (Kaiho et al., 2016). Therefore, I use each SST anomaly at low latitudes as an intermediate value (near average) in the Earth at each age. The error for the SST anomaly in geologic ages is approximately ± 1 °C, approximately ± 0.5 °C depending on the sample location to obtain the average value and approximately ± 0.5 °C depending on detection of the largest anomaly for abrupt short-term events from sedimentary rocks, which usually deposited 1–100 mm/kyr, except for impact ejecta sediment. I converted SST anomalies of various geologic ages to global surface temperature anomalies and land-surface temperature anomalies using Fig. 1d, which was generated from global cooling and warming (recovery) data of the climate model calculation (Kaiho and Oshima, 2017) (Fig. 1d).

2.3 Relationships between taxa loss % and temperature anomaly

Finally, I show correlation coefficient R between taxa loss % and absolute habitat temperature (sea surface for marine faunas and land surface for terrestrial faunas) for the three marine genera loss percentage data sets and a terrestrial data set. To calculate their correlation coefficient, marine end-G and H–A data are included into each data set, because the small percentage values cannot be changed largely due to the method variation (Table 3).

Table 2: Source latitudes of causal gas and aerosols and SST data

Crisis	Source of causal gas and aerosols	SST data site
K–Pg	~25°N	~30°N
end-T	~20°S – ~30°N	~30°N
end-P	~50°N	~15°N
end-G	~30°N	~30°N
F–F	~10°S – ~30°N	~25°S
end-O	?	~20°S – ~10°S

O: Ordovician. F–F: Frasnian–Famennian boundary. G: Guadalupian. P: Permian. T: Triassic. K–Pg: Cretaceous–Paleogene boundary.

Table 3: Marine and terrestrial genera and species extinction %, absolute SST anomaly and land temperature anomaly, and their correlation coefficient *R* for Figure 3

Crisis	Marine Sepkosky M genus Ext (%)	Marine Sepkosky M species Ext (%)	Marine Bambach M genus Ext (%)	Marine Bambach M species Ext (%)	Marine Stanley M genus Ext (%)	Marine Stanley M species Ext (%)	Absolute SST anomaly (°C)	Tetrapod Genus genus Ext (%)	Tetrapod species species Ext (%)	Absolute land Temperature anomary (°C)
H–A	0	0	0	0	0	0	*0.7*	*0.6*	*1*	*1.5*
K–Pg	45	72	40	68	39	68	7	39	67	*16*
End-T	46	73	43	70			6	41	70	*13*
End-P	66	86	56	80	62	83	10	89	97	*22*
End-G	5	11	5	11	5	11	4	31	*38*	*9*
F–F	41	69	35	62	18	42	5	-	-	*11*
End-O	52	77	40	68	45.5	72	7	-	-	*16*
Correlation *R*	0.92	0.88	0.92	0.88	0.95	0.95		0.95	0.98	

Bold roman marine taxa extinction % data are from Sepkoski (2006) in Sepkoski M column, Bambach (2006) in Bambach M (method) column, and Stanley (2016) in Stanley M column. Data marked by light letters of extinction % are from Fan et al. (2020) for End-G, Barnosky et al. (2011) and Ceballos et al. (2015) for H–A. Italic values are converted using Figure 1b–d. See Table 1 for the other explanations.

3 Results

3.1 Magnitude of marine/terrestrial crises

My analysis of the major mass extinctions shows that the Late Ordovician mass extinction (LOME) was marked by only a marine crisis (40–52 % genera loss and 68–77 % species loss in the two methods) since terrestrial tetrapods had not yet appeared. The Late Devonian mass extinction (LDME) resulted in the loss of 18–41 % genera and 42–69 % species for marine animals at the Frasnian–Famennian boundary (F–F) (I ignored the tetrapod extinction percentage due to the very low apparent diversity) (Kaiho et al., 2016). The last three major mass extinctions, end-Permian, end-Triassic, and Cretaceous–Paleogene (K–Pg) boundary, were characterized by high extinction percentages of both marine and terrestrial genera (marine: 56–66 %, 43–46 %, and 39–45 %; terrestrial: 89 %, 41 %, and 39 %; Fig. 2, Table 1) and species (marine: 80–86 %, 70–73 %, and 68–72 %; terrestrial: 97 %, 70 %, 67 %; Fig. 2, Table 1). In total, the five major mass extinctions were marked by high marine genera and species extinction percentages (18–62 % and 35–83 %). However, the end-Guadalupian extinction was marked by low marine genera and species loss (5 % and 11 %) and higher terrestrial genera and species loss (31 % and 38 %), corresponding to a major terrestrial crisis, not a major mass extinction, accompanied by a large reduction in shallow marine fusulinids (Feng et al., 2020) and reef animals (Fluegel and Kiessling, 2002) due to terrestrial disturbance. The Paleozoic biotic crises during global warming following the diversification of tetrapods had higher extinction percentages of terrestrial animals than of marine animals, but the Mesozoic biotic crises during global cooling had similar percentages of terrestrial and marine animals.
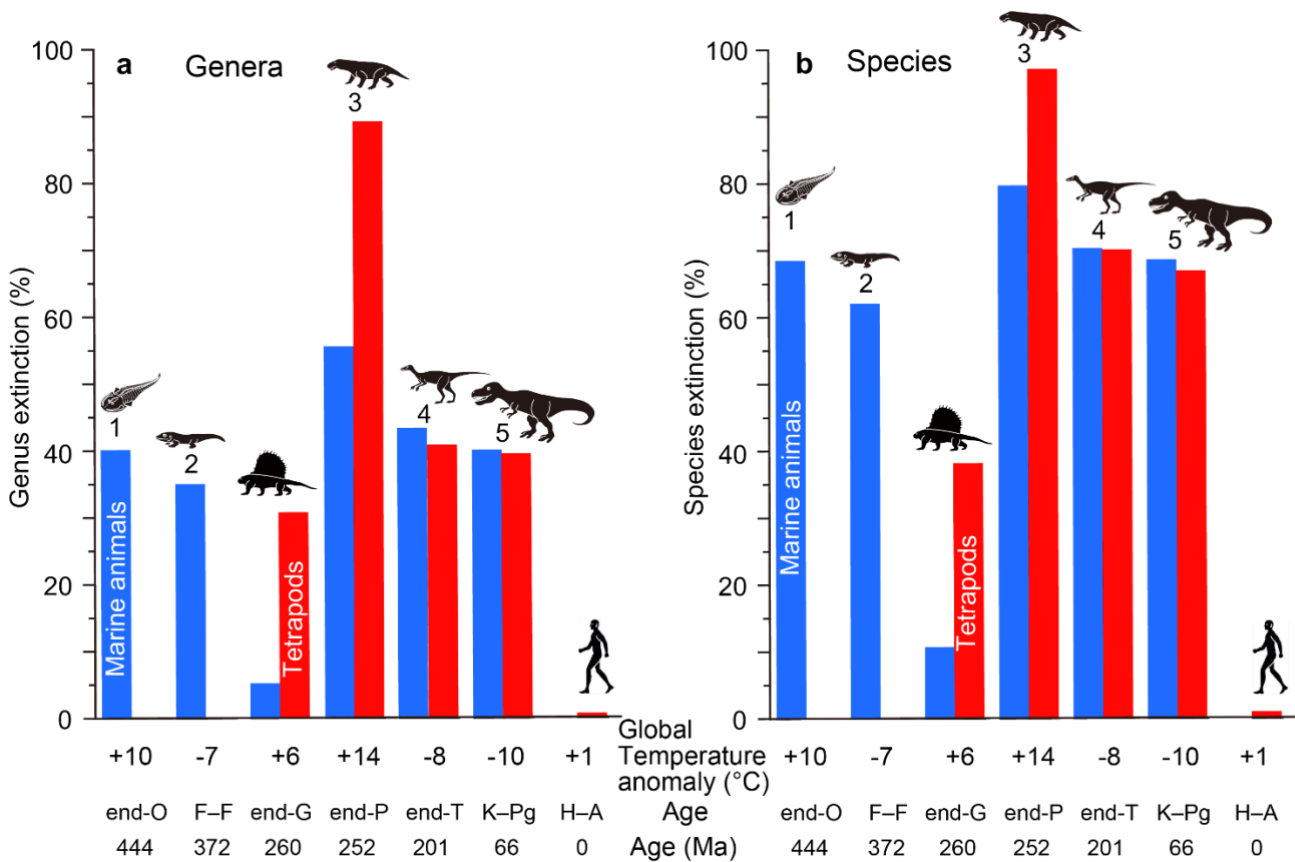
Figure 2: Genera (**a**) and species (**b**) extinction percentages of marine animals and tetrapods for major mass extinctions and the end-Guadalupian and Holocene–Anthropocene crises. All data are from Table 1. Marine genus and species extinction values shown by blue columns based on Bambach (2006) for genera and my calculation using Fig. 1b for species. Terrestrial genus and species extinction values shown by red columns based on Benton et al. (2013) and Sahney and Benton (2017) for genera and my calculation using Fig. 1b for species. These extinction % data are comparable because of usage of similar methods (conventional method and substage intervals). Global temperature anomaly: Global surface temperature anomaly. O: Ordovician. F–F: Frasnian–Famennian boundary. G: Guadalupian. P: Permian. T: Triassic. K–Pg: Cretaceous–Paleogene boundary. H–A: Holocene–Anthropocene (1850 to 2010 on going). Numbers 1 to 5: five major mass extinction. Each silhouette shows a representative vertebrate animal from each age.

3.2 Sea-surface temperature anomaly during crises

There are two extinction levels on the LOME at the Katian−Hirnantian boundary (445.2 Ma) and late Hirnantian (~444 Ma) (Bond and Grasby, 2020). Between the two extinctions, global cooling occurred, as evidenced by conodont apatite oxygen isotopes and glacial deposits (Finnegan et al., 2011); however, the two extinction levels coincided with the two shorter-term global warming events based on the oxygen isotope data of conodont apatite (Bond and Grasby, 2020). I select the maximum

7

anomaly +7 °C SST (~10^5 years) from the data of Finnegan et al. (2011) for the LOME. The trigger is estimated to be volcanism as evidenced by coincidental mercury concentration for LOME (Jones et al., 2017; Bond and Grasby, 2020).

The LDME is composed of the Frasnes, Kellwasser, and Hangenberg crises at 383, 372, and 359 Ma, respectively, and the Kellwasser is the largest crisis (Barash, 2016). The trigger was the large igneous province (LIP) emplacement of Viluy and PDD LIPs, as evidenced by mercury and coronene concentrations (Racki, 2020; Kaiho et al., 2021b). I use the largest abrupt cooling marked by a -5 °C SST anomaly (~10^4 years) at the Lower Kellwasser and the Upper Kellwasser crises from the oxygen isotope data of conodont apatite of Balter et al. (2008) for LDME, whereas the long-term gradual SST change between the crises shows global warming (+6 °C SST anomaly in 5 x 10^5 years).

The Late Guadalupian crisis (LGC) occurred in the mid-Capitanian, 262 Ma, followed by the Guadalupian–Lopingian (G−L) boundary event at 259 Ma (Chen and Xu, 2019). The coincidental volcanic eruptions of the Emeishan Large Igneous Province (ELIP) in South China are thought to be the trigger of the crisis (Chen and Xu, 2019), as evidenced by mercury concentration peaks beginning in the mid-Capitanian and peaking during the G−L transition (Grasby et al., 2016). The largest abrupt anomaly +4 °C SST (~10^5 years) coinciding with the volcanism and extinction at the G−L boundary from the data of Chen et al. (2011) is used for LGC.

The largest biodiversity loss in the Phanerozoic occurred at the end of the Permian, with local extinction during the earliest Triassic, ~252.0–251.9 million years ago (Song et al., 2013; Kaiho et al., 2021a), marking the end of the Paleozoic. The LIP in Siberia caused sill emplacement and large eruptions at that time (Burgess et al., 2017). The coincidence of volcanic eruption and the biotic crisis was shown using the correlation of mercury, coronene, and coal fly ash (Grasby et al., 2011, 2013; Kaiho et al., 2021a). I use the largest anomaly +10 °C SST (2 x 10^4 years) from just before the mass extinction (Bed 24) to the first minimum $\delta^{18}O$apatite value (base of Bed 27) at GSSP Meishan based on new conodont apatite $\delta^{18}O$ data showing the 2.5 permil anomaly of Chen et al. (2016) for the end-Permian mass extinction (EPME).

The age of the end-Triassic mass extinction (ETME) is estimated to be 201.564 ± 0.015 Ma, which corresponds to the emplacement of the Central Atlantic Magmatic Province (CAMP, 201.6 to 201.0 Ma) (Davies et al., 2017). The SST anomaly during the crisis is estimated as -6 °C (~10^3 years cooling during ~10^4-years) from the averaged $\delta^{18}O$ of oyster shells, assuming stable salinity, which was followed by long-term (2 x 10^5 years) global warming (Korte et al., 2009; Kaiho et al., 2022). There were no crises during the long-term warming (Kaiho et al., 2022). I use the -6 °C anomaly for ETME, indicating global cooling.

Only the K–Pg mass extinction (KPME) at 66 Ma occurred as the result of an asteroid impact (Schulte et al., 2010). This impact produced large amounts of soot and sulfuric acid aerosols in the stratosphere by the ignition and melting of sedimentary rocks (Kaiho et al., 2016; Kaiho and Oshima, 2017). Stratospheric aerosols efficiently absorb and scatter solar radiation and reduce sunlight reaching the Earth's surface, which induces strong global cooling and a significant decrease in precipitation, particularly over equatorial areas, over ten years, with the maximum occurring in the second year (Kaiho et al., 2016; Kaiho and Oshima, 2017). Organic biomarker TEX$_{86}$ values show -7 °C as the SST largest absolute anomaly during the crisis (Vellekoop et al., 2014). This SST anomaly is consistent with the -10 °C global cooling estimated by climate model

calculations and the survival of equatorial crocodilians (Kaiho et al., 2016). The global cooling duration is ~10 years based on impact-induced climate model calculations (Kaiho et al., 2016; Kaiho and Oshima, 2017). When the Deccan Traps volcanism also contributed to the global cooling the duration could have been longer ($10–10^2$ years) for one pulse (Schmidt, 2016).

200

3.3 Relationship between extinction magnitudes and surface temperature anomalies

I compare those data on each biotic crisis based on an assumption that the Earth and contemporary life at the time of each crisis are themselves more-or-less comparable through time. My results for the relationship between past mass extinctions and surface temperature anomalies show the following features. A 4 °C SST warming was detected at the end of the
205 Guadalupian (Chen et al., 2011), equivalent to 9 °C warming on land (6 °C global warming), as shown in Fig. 1d, which corresponded to 5% and 11% marine genera and species extinction and 31% and 38% terrestrial genera and species extinction, respectively (Figs. 3a, 3d; Table 1). The end-Ordovician mass extinction had higher temperature anomalies and higher extinction percentages (40–46 % and 68–72 % marine genera and species, respectively). The EPME was marked by the highest temperature anomalies (10 °C SST [Chen et al., 2016], 22 °C on land, and 14 °C global warming) and the highest
210 extinction percentages (56–62 % and 80–83 % marine genera and species and 89 % and 97 % terrestrial tetrapod genera and species, respectively). In contrast, the Frasnian–Famennian (F–F) boundary, the end-Triassic and Cretaceous–Paleogene (K–Pg) boundary mass extinctions coincided with the 5 °C, 6 °C, and 7 °C SST (Balter et al., 2008; Korte et al., 2009; Vellekoop et al., 2014) cooling corresponding to 11 °C ,13 °C, and 16 °C cooling on land and 7 °C, 8 °C and 10 °C global cooling (Fig. 1). The F–F crisis corresponds to 18–35 % and 42–62 % marine genera and species loss, respectively, that is, a
215 marine crisis and the smallest major mass extinction, respectively. The ETME correlated with 43 % and 70 % marine genera and species loss and 41 % and 70 % terrestrial tetrapod genera and species loss, respectively, and the KPME correlated with 39–40 % and 68 % marine genera and species loss and 39 % and 67% terrestrial tetrapod genera and species loss, respectively (Figs. 3a, d). These results indicate that a larger absolute value of the global temperature anomaly corresponds to a higher extinction percentage in the marine and terrestrial realms, regardless of whether the change is due to global
220 warming or global cooling, considering a ± 5 % error (Figs. 3c, f). The correlation coefficient R between marine extinction % and absolute SST anomaly is 0.92–0.95 for genus and 0.88– 0.95 for species, and that between terrestrial extinction % and absolute land temperature anomaly is 0.95 for genus and 0.98 for species (Figs. 3c, 3f, Table 3). There is little or no difference to R for marine animals in the three data sets. Differences in methods do not affect the conclusions. These new data indicate that global warming temperatures (> 9 °C) inducing major mass extinctions is likely higher than that
225 of global cooling (> 7 °C). These relationships indicate that abrupt temperature anomalies and coincidental environmental changes associated with high energy input by volcanism and impact relate to the magnitude of mass extinctions.
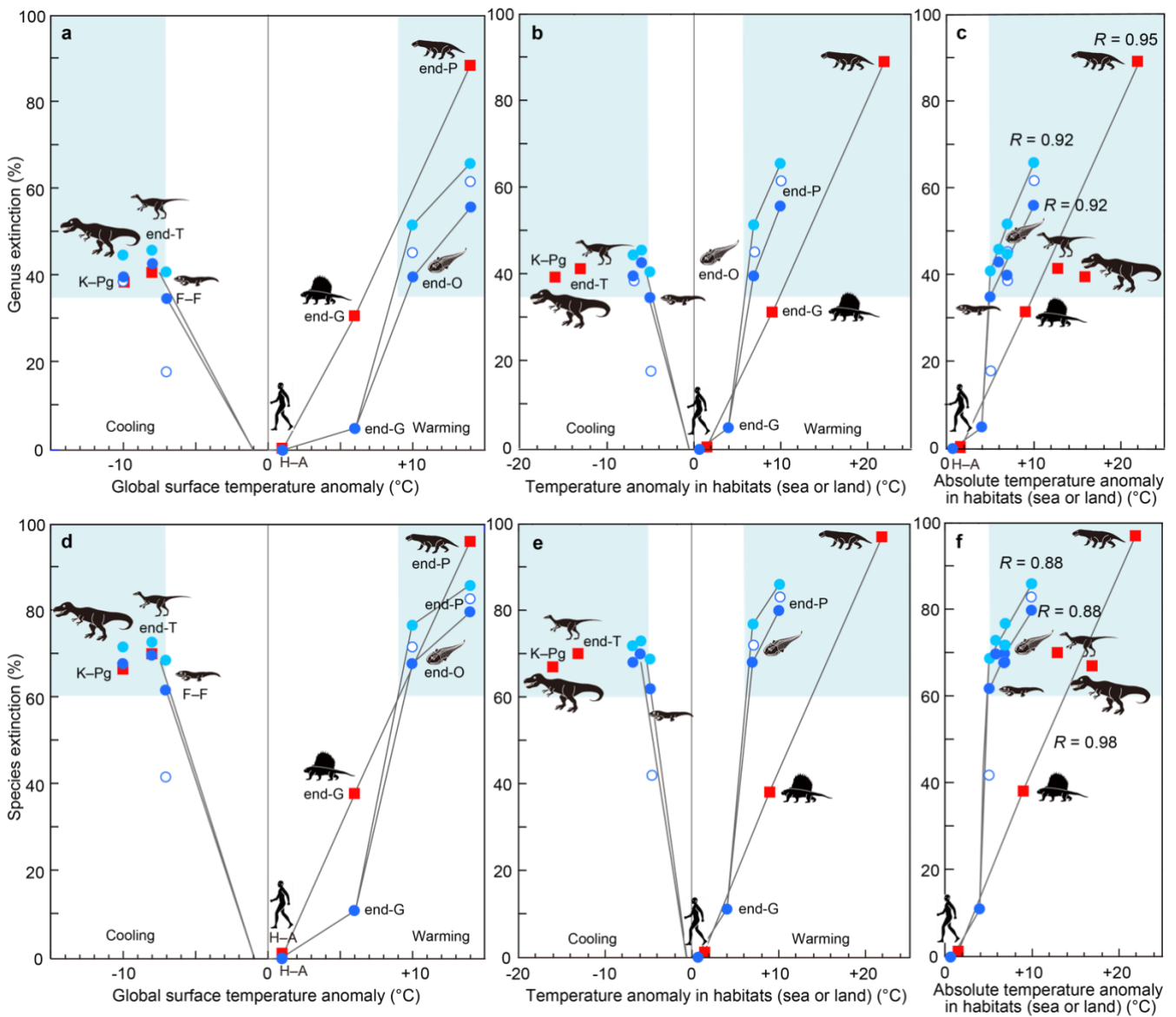
9

Figure 3: Relationship between genera and species extinction percentage and surface temperature anomaly in major mass extinctions, the end-Guadalupian crisis, and the current crisis in the Anthropocene. All vertical axes show genus or species extinction (%). (**a**)–(**c**): genera extinction. (**d**)–(**f**): species extinction. (**a**) and (**d**): relationship between that and global surface anomaly. (**b**) and (**e**): relationship between that and surface temperature anomaly in habitats (global sea or land). (**c**) and (**f**): relationship between that and absolute surface temperature anomaly in habitats (global sea or land). Blue circles: marine extinctions [light blue solid circles: Sepkoski (1996; conventional method and 107 interval data) and data of end-G and H–A; blue solid circle: Bambach (2006; conventional method and 165 substage interval data), open circle: Stanley (2016; new method and substage interval data)]. Red squares: terrestrial extinctions represented by tetrapods (calculated

10

from data of Benton et al. (2013; substage intervals) for end-O, F–F, end-P, end-T and Sahney et al. (2017) for K–Pg. All data are from Table 3. Comparable data sets are blue solid circles and red squares due to similar methods (conventional method and substage interval data). Pale blue areas show major extinctions. O: Ordovician. F–F: Frasnian–Famennian boundary. G: Guadalupian. P: Permian. T: Triassic. K–Pg: Cretaceous–Paleogene boundary. H–A: Holocene–Anthropocene.

240   I also show correlation coefficient R between marine extinction % and absolute SST anomaly and that between terrestrial extinction % and absolute land temperature anomaly based on the conventional method.

4. Discussion

4.1 Summary and interpretation on extinction–temperature relationship

245   I studied only biotic crises showing coincidence of surface temperature change and an extinction, resulting in a very high correlation coefficient between absolute SST anomaly and extinction magnitude on marine fossils in three data sets based on the three methods of Sepkosky, Bambach, and Stanley (R = 0.92, 0.92 and 0.95 for genus). That of Song et al. (2021) is much lower (R = 0.63 for genus), which is likely due to the usage of extinctions having an uncertain coincidence with global climate changes.

250   When summarizing and interpreting these results for the past six representative crises, I find that (i) higher global surface temperature anomalies correspond to higher extinction percentages in both marine and terrestrial realms, respectively (Figs. 3a, 3d), which suggests that climate change and related or coincidental environmental destruction is the main cause of mass extinctions; (ii) >35 % genera and >60 % species loss correspond to > +9 °C global warming and < -7 °C global cooling, respectively (Figs. 3a, 3d); (iii) higher extinction percentages appear in the terrestrial realm (tetrapods) than in the

255 marine realm (invertebrate) under the same global temperature anomaly in warming events (Figs. 3a, 3d) because the ratio of the surface temperature anomaly in the terrestrial realm to that in the marine realm is 2.2 (Fig. 1d); (iv) similar extinction percentages appear in the terrestrial realm (tetrapods) and the marine realm (invertebrate) in cooling events (Figs. 3a, 3d); (v) marine animals are more likely to become extinct under a lower habitat temperature anomaly than tetrapods regardless of the difference between warming and cooling (Figs. 3c, 3f); and (vi) a similar absolute habitat temperature anomaly corresponds

260 to a similar extinction magnitude in marine invertebrates and terrestrial tetrapods, respectively (Figs. 3c, 3f).

     Song et al. (2021) concluded that a temperature increase of 5.2 °C above the pre-industrial level at the present rate of increase would likely result in a major marine mass extinction. The 5.2 °C is SST anomaly, which corresponds to a 7 °C global surface temperature anomaly. This is roughly consistent with my results shown in Figure 3, but absolute temperature anomalies of global warming inducing major mass extinctions are likely higher by 2 °C compared to global cooling

265 anomalies.

     Major terrestrial crises occur under lower global temperature anomalies than major marine crises in the Paleozoic (Figs. 3a, 3d), which implies that major terrestrial crises must have occurred more frequently than major marine crises in the Paleozoic. Evidence for this difference is nine decreases in tetrapod diversity having ≥ 35 % genus loss during the late Carboniferous to Early Jurassic (Benton et al., 2013) compared with two marine crises having ≥ 35 % genus extinctions

270   during the same interval (end-Permian, end-Triassic). On the other hand, marine animals are more likely to become extinct under lower habitat temperature anomalies than tetrapods (Figs. 3b, 3e), which is consistent with a higher sensitivity of marine animals to warming than terrestrial animals based on the current global temperature and thermal tolerance data (Pinsky et al., 2019). The physical law of the temperature anomaly extinction relationship shown in Figs. 1d and 3 controls the extinction of terrestrial and marine animals, as shown in Fig. 2.

275

4.2 Climate changes and causes of mass extinctions

    McPherson et al. (2022) argued that slow temperature changes will provide opportunities for species to adapt, thus, the rapidity of environmental change produced by abrupt climate change is fundamentally more important than the magnitude of the change alone for mass extinctions. The duration of global cooling and warming of the large volcanic eruptions during the five crises were 10^4 years and 10^4–10^5 years, respectively. In the case of the cooling crises, much shorter climate change events could have repeatedly occurred because one large eruption causes a ~10-year global cooling pulse (Timmreck et al., 2012). For example, a 10^4-year cool-climate-period corresponding to the end-Triassic mass extinction likely contained numerous cooling pulses causing the 6 °C SST reduction over <10^3 years in total (Kaiho et al., 2022). Thus volcanic eruptions cause repeated abrupt (10 years) global cooling pulses, whereas a bolide impact would cause only one cooling
285   pulse of ~10 years. Global warming lasts 10^4–10^5 years in the case of volcanic events. Coincidental environmental changes should relate to the magnitude of mass extinctions.

    The significant relationship between the surface temperature anomaly and extinction magnitude indicates that the cause of major extinctions is surface temperature change and coincidental environmental changes, such as acid rain, ozone depletion, reducing sunlight, desertification, soil erosion, and oceanic anoxia, driven by large volcanic eruptions and
290   projectile impacts; these causal climatic and environmental conditions changed in parallel due to the same controls as each volcanism and impact. These climatic and environmental anomalies are controlled by stratospheric aerosols, such as sulfuric acid and black carbon, for reducing sunlight – global cooling – acid rain, halogen for ozone depletion, and atmospheric greenhouse gases, such as CO_2 and methene, for surface warming.

    Global cooling and warming have been reported in many periods in the Phanerozoic based on oxygen isotopes (Stanley,
295   2010); however, most of them are long-term climate changes. When surface temperature changes slowly (>~10^3 years), animals migrate and survive; an abrupt temperature change and accompanied environmental change is thought to be essential for mass extinctions. There were no significant marine extinctions during global warming of two famous global warming events at the end-Cenomanian and Paleocene–Eocene transitions (Kaiho, 1994); which were due to volcanism under the oceanic crust (Bond and Wignall, 2014). This type of volcanism cannot eject volcanic SO_2 gas into the stratosphere, resulting
300   in no short-term global cooling and gradual global warming by the gradual release of CO_2 from volcanism under the ocean; conversely, the Late Devonian, end-Permian, and end-Triassic LIPs were emplaced on land, resulting in SO_2 gas emissions into the stratosphere, causing short-term global cooling and accompanying environmental changes, followed by longer-term global-warming due to volcanic greenhouse gas emissions. An eruption causes global cooling that lasts for a few to ten

years; thus, detection is difficult; however, LIP volcanism causes thousands of eruptions (Svensen et al., 2009), resulting in
305   the detection of decreases in SST from sedimentary rocks when the release of SO_2 gas to the stratosphere exceeds $>10^3$ years (Kaiho et al., 2022), but no detection occurs in cases of $< 10^2$-year SO_2 emissions. Global cooling is followed by global warming due to the cessation of SO_2 release to the stratosphere and the accumulation of CO_2 in the atmosphere from volcanisms (Kaiho et al., 2022). Global warming lasts for a long time (usually 10^4–10^5 years), resulting in easy detection.

Global warming has been detected in some volcanic and impact cases, whereas global cooling has been detected from
310   (i) sedimentary rocks formed under volcanism characterized by massive SO_2 gas emissions and relatively low CO_2 emissions by low-temperature volcanism to the stratosphere (ETME) (Kaiho et al., 2022) and (ii) quickly deposited impact ejecta (Vellekoop et al., 2014) near the impact crater in an impact case (KPME). There is a possibility of undetected short-term global cooling before global warming in the other volcanism-induced major biotic crises. Larger volcanisms generally cause larger SO_2, CO_2, and halogen emissions, which could have resulted in a significant relationship between the global warming
315   temperature anomaly and extinction magnitude, even if the real main cause of crises is reduced sunlight – global cooling – acid rain, ozone depletion or oceanic anoxia. Therefore, the relationship between the absolute temperature anomaly and extinction magnitude is shown in Figs. 3c and 3f. The significant relationship in marine and terrestrial animals clarified in this study indicates that the global climate and the accompanying environmental changes are related to the magnitude of mass extinctions.
320

5. Conclusions

I conclude that (i) the magnitude of major extinctions in marine invertebrates and that of terrestrial tetrapods corresponds to the coincidental abrupt anomaly of global surface temperature, respectively; (ii) > 35 % genera and > 60 % species loss correlate to > 7 °C global cooling and > 9 °C global warming; (iii) there is a significant relationship ($R = 0.92$–
325   0.95) between extinction magnitude of marine invertebrates and absolute SST anomaly as well as that of terrestrial tetrapods and absolute land-surface temperature anomaly ($R = 0.95$–0.98); (iv) marine animals become extinct under a lower habitat temperature anomaly than tetrapods regardless of the difference between warming and cooling, which is likely due to a higher sensitivity of marine animals than terrestrial animals. These relationships indicate that abrupt temperature anomalies and coincidental environmental changes associated with abrupt high energy input by LIP volcanism and that an asteroid
330   impact relates to the magnitude of mass extinctions.

Data and materials availability: All data is available in the main text.

References

Balter, V., Renaud, S., Girard, C., and Joachimski, M. M.: Record of climate-driven morphological changes in 376 Ma
340   Devonian fossils, Geology, 36, 907–910, doi: 10.1130/G24989A.1, 2008.

Bambach, R. K.: Phanerozoic biodiversity mass extinctions, Ann. Rev. Ear. Planet. Sci. 34, doi:
        10.1146/annurev.earth.33.092203.122654, 127–155, 2006.

Barash, M. S.: Causes of the great mass extinction of marine organisms in the Late Devonian, Oceanology, 56, 863–875, doi:
        10.1134/S0001437016050015, 2016.

345 Barnosky, A. D., Hadly, E. A., Gonzalez, P., Head, J., Polly, P. D., Lawing, A. M., Eronen, J. T., Ackerly, D. D., Alex, K.,
        Biber, E., Blois, J., Brashares, J., Ceballos, G., Davis, E., Dietl, G.P., Dirzo, R., Doremus, H., Fortelius, M., Greene, H.
        W., Hellmann, J., Hickler, T., Jackson, S. T., Kemp, M., Koch, P. L., Kremen, C., Lindsey, E. L., Looy, C., Marshall, C.
        R., Mendenhall, C., Mulch, A., Mychajliw, A. M., Nowak, C., Ramakrishnan, U., Schnitzler, J., Das Shrestha, K., Solari,
        K., Stegner, L., Stegner, M. A., Stenseth, N. C., Wake, M. H., Zhang, Z.: Has the Earth's sixth mass extinction already
350   arrived?, Nature, 471, 51–57, doi:10.1038/nature09678, 2011.

Benton, M. J., Ruta, M., Dunhill, A. M., and Sakamoto, M.: The first half of tetrapod evolution, sampling proxies, and fossil
        record quality, Palaeogeogr. Palaeoclimatol. Palaeoecol., 372, 18–41, http://dx.doi.org/10.1016/j.palaeo.2012.09.005,
        2013.

Bond, D. P. G. and Grasby, S. E.: Late Ordovician mass extinction caused by volcanism, warming, and anoxia, not cooling
355   and glaciation, Geology, 48, 777–781, https://doi.org/10.1130/G47377.1, 2020.

Bond, D. P. G. and Wignall, P. B.: "Large igneous provinces and mass extinctions: An update" in Volcanism, Impacts, and
        Mass Extinctions: Causes and Effects, Keller, G. and Kerr, A. C., Eds. (Geol. Soc. Am. Spec. Pap. 505, https://
        doi .org/10.1130/2014.2505(02), 2014).

Burgess, S. D., Muirhead, J. D., and Bowring, S.: Initial pulse of Siberian Traps sills as the trigger of the end-Permian mass
360   extinction, Nat. Comm., 8, 15596, doi: 10.1038/s41467-017-00083-9, 2017.

Ceballos, G., Ehrlich, P. R., Barnosky, A. D., García, A., Pringle, R. M., and Palmer, T. M., Accelerated modern human-
        induced species losses: Entering the sixth mass extinction, Sci. Adv. 1, e1400253, 10.1126/sciadv.1400253, 2015.

Chen, B., Joachimski, M. M., Sun, Y. D., Shem, S. Z., and Lai, X. L.: Carbon and conodont apatite oxygen isotope records
        of Guadalupian-Lopingian boundary sections: Climatic or sea-level signal?, Palaeogeogr., Palaeoclimatol., Palaeoecol.,
365   311, doi:10.1016/j.palaeo.2011.08.016, 145–153, 2011.

Chen, J., Shen, S., Li, X., Xu, Y., Joachimski, M. M., Bowring, S. A., Erwin, D. H., Yuan, D., Chen, B., Zhang, H., Wang,
        Y., Cao, C., Zheng, Q., and Mu, L.: High-resolution SIMS oxygen isotope analysis on conodont apatite from South
        China and implications for the end-Permian mass extinction, Palaeogeogr. Palaeoclimatol. Palaeoecol. 448, 26–38, doi:
        10.1016/j.palaeo.2015.11.025, 2016.

370 Chen, J. and Xu, Y., Establishing the link between Permian volcanism and biodiversity changes: Insights from geochemical proxies, Gondwana Res., 75, 68–96, https://doi.org/10.1016/j.gr.2019.04.008, 2019.

Davies, J. H. F. L., Marzoli, A., Bertrand, H., Youbi, N., Ernesto, M., and Schaltegger, U.: End-Triassic mass extinction started by intrusive CAMP activity, Nat. Comm. 8, 15596, doi:10.1038/ncomms15596, 2017.

Fan, J., Shen, S., Erwin, D. H., Sadler, P. M., MacLeod, N., Cheng, Q., Hou, X., Yang, J., Wang, X., Wang, Y., Zhang, H.,
375 Chen, X., Li, G., Zhang, Y., Shi, Y., Yuan, D., Chen, Q., Zhang, L., Li, C., and Zhao, Y.: A high-resolution summary of Cambrian to Early Triassic marine invertebrate biodiversity, Science, 10.1126/science.aax4953, 367, 272–277, 2020.

Feng, Y., Song, H., Bond, D. P. G.: Size variations in foraminifers from the early Permian to the Late Triassic: implications for the Guadalupian–Lopingian and the Permian–Triassic mass extinctions, Paleobiology, 46, 511–532, doi: 10.1017/pab.2020.37, 2020.

380 Finnegan, S., Bergmann, K., Eiler, J. M., Jones, D. S., Fike, D. A., Eisenman, I., Hughes, N. C., Tripati, A. K., and Fischer, W. W.: The magnitude and duration of Late Ordovician-Early Silurian Glaciation, Science, 331, 903–906, 10.1126/science.1200803, 2011.

Fluegel, E. and Kiessling, W.: Patterns of Phanerozoic reef crises. SEPM (Society for Sedimentary Geology) Spec. Pub. 72, 691–733, doi: 10.2110/pec.02.72.0691, 2002.

385 Grasby, S. E., Beauchamp, B., Bond, D. P. G., Wignall, P. B., and Sanei, H., Mercury anomalies associated with three extinction events (Capitanian Crisis, Latest Permian Extinction and the Smithian/Spathian Extinction) in NW Pangea, Geol. Mag., 153, 285–297, doi:10.1017/S0016756815000436, 2016.

Grasby, S. E., Sanei, H., Beauchamp, B., and Chen, Z. H.: Mercury deposition through the Permo-Triassic biotic crisis, Chem. Geol., 351, 209–216, http://dx.doi.org/10.1016/j.chemgeo.2013.05.022, 2013.

390 Grasby, S. E., Sanei, H., and Beauchamp, B.: Catastrophic dispersion of coal fly ash into oceans during the latest Permian extinction, Nat. Geosci., 4, 104–107, www.nature.com/naturegeoscience, 2011.

Huang, Y., Chen, Z.-Q., Wignall, P. B., Grasby, S. E., Zhao, L., Wang, X., and Kaiho, K.: Biotic responses to volatile volcanism and environmental stresses over the Guadalupian-Lopingian (Permian) transition, Geology, 47, 175–178, doi: 10.1130/G45283.1, 2019.

395 IUCN 2021, The IUCN Red List of Threatened Species, Version 2021-1, https://WWW.iucnredlist.org., 2021.

Jones, D. S., Martini, A. M., Fike, D. A., and Kaiho, K.: A volcanic trigger for the Late Ordovician mass extinction? Mercury data from south China and Laurentia, Geology, 45, 631–634, https://doi.org/10.1130/G38940.1, 2017.

Kaiho, K.: Planktonic and benthic foraminiferal extinction events during the last 100 m.y., Palaeogeogr., Palaeoclimatol., Palaeoecol., 111, 45–71, 10.1016/0031-0182(94)90347-6,1994.

400 Kaiho, K., Aftabuzzaman, M., Jones, D. S., and Tian, L.: Pulsed volcanic combustion events coincident with the end-Permian terrestrial disturbance and the following global crisis, Geology, 49, 289−293, https://doi.org/10.1130/G48022.1, 2021a.

Kaiho, K., Miura, M., Tezuka, M., Hayashi, N., Jones, D. S., Oikawa, K., Casier, J.-G., Fujibayashi, M., and Chen, Z.-Q.:

Coronene, mercury, and biomarker data support a link between extinction magnitude and volcanic intensity in the Late
405   Devonian, Glob. Planet. Chang., 103452, https://doi.org/10.1016/j.gloplacha.2021.103452, 2021b.

Kaiho, K. and Oshima. N.: Site of asteroid impact changed the history of life on Earth: the low probability of mass
extinction, Sci. Rep., 7, 14855, DOI:10.1038/s41598-017-14199-x, 2017.

Kaiho, K., Oshima, N., Adachi, K., Adachi, Y., Mizukami, T., Fujibayashi, M., and Saito, R.: Global climate change driven
by soot at the K–Pg boundary as the cause of the mass extinction, Sci. Rep., 6, 28427, doi:10.1038/srep28427, 2016.

410   Kaiho, K., Tanaka, D., Richoz, S., Jones, D. S., Saito, R., Kameyama, D., Ikeda, M., Takahashi, S., Aftabuzzaman, M., and
Fujibayashi, M.: Volcanic temperature changes modulated volatile release and climate fluctuations at the end-Triassic
mass extinction, Earth Planet. Sci. Lett., 579, 117364, https://doi.org/10.1016/j.epsl.2021.117364, 2022.

Korte, C., Hesselbo, S. P., Jenkyns, H. C., Rockaby, R. E., and Spoetl, C.: Palaeoenvironmental significance of carbon- and
oxygen-isotope stratigraphy of marine Triassic–Jurassic boundary sections in SW Britain, J. Geol. Soc., 166, 431–445,
415   doi: 10.1144/0016-76492007-177, 2009.

McPherson, G. R., Sirmacek, B., Vinuesa, R.: Environmental thresholds for mass-extinction events, Results in Engineering,
13, 100342, https://doi.org/10.1016/j.rineng.2022.100342, 2022.

Pinsky, M. L., Eikeset, A. M., McCauley, D. J., Payne, J. L., and Sunday, J. M.: Greater vulnerability to warming of marine
versus terrestrial ectotherms, Nature, 569, 108–111, https://doi.org/10.1038/s41586-019-1132-4, 2019.

420   Racki, G.: A volcanic scenario for the Frasnian–Famennian major biotic crisis and other Late Devonian global changes:
More answers than questions?, Glob. Planet. Chang., 189, 103174, https://doi.org/10.1016/j.gloplacha.2020.103174,
2020.

Rampino, M. R., Caldeira, K., and Zhu, Y.: A 27.5-My underlying periodicity detected in extinction episodes of non-marine
tetrapods, Hist. Biology, 33, 3084–3090, https://doi.org/10.1080/08912963.2020.1849178, 2020.

425   Rampino, M. R. and Shen, S-Z.: The end-Guadalupian (259.8 Ma) biodiversity crisis: the sixth major mass extinction?,
Historical Biol., 33, 1–7, https://doi.org/10.1080/08912963.2019.1658096, 2019.

Raup, D. M.: Size of the Permo-Triassic bottleneck and its evolutionary implications, Science, 206, 217–218, doi:
10.1126/science.206.4415.217, 1979.

Sahney, S. and Benton, M. J.: The impact of the Pull of the Recent on the fossil record of tetrapods, Evol. Ecol. Res., 18,
430   2017.

Sahney, S., Benton, M. J., and Ferry, P. A.: Links between global taxonomic diversity, ecological diversity, and the
expansion of vertebrates on land, Biol. Lett., 6, 544–547, http://dx.doi.org/10.1098/rsbl.2009.1024, 2010.

Schulte, P., Alegret, L., Arenillas, I., Arz, J. A., Barton, P. J., Bown, P. R., Bralower, T. J., Christeson, G. L., Claeys, P.,
Cockell, C. S., Collins, G. S., Deutsch, A., Goldin, T. J., Goto, K., Grajales-Nishimura, J. M., Grieve, R. A. F., Gulick, S.
435   P. S., Johnson, K. R., Kiessling, W., Koeberl, C., Kring, D. A., MacLeod, K. G., Matsui, T., Melosh, J., Montanari, A.,
Morgan, J. V., Neal, C. R., Nichols, D. J., Norris, R. D., Pierazzo, E., Ravizza, G., Rebolledo-Vieyra, M., Reimold, W.
U., Robin, E., Salge, T., Speijer, R. P., Sweet, A. R., Urrutia-Fucugauchi, J., Vajda, V., Whalen, M. T., and Willumsen,

16

P. S.: The Chicxulub asteroid impact and mass extinction at the Cretaceous−Paleogene boundary, Science, 327, 1214–1218, 10.1126/science.1177265, 7–23, 2010.

440 Sepkoski, J. J., Jr.: Mass extinctions in the Phanerozoic oceans: A review, Geological Implications of Impacts of Large Asteroids and Comets on the Earth, in edited by Silver, L. T. and Schultz, Geol. Soc. Am. Spec. Pap., 190, 283–289, 1982.

Sepkoski, J. J., Jr.: Phanerozoic overview of mass extinction. Patterns and Processes in the History of Life, edited by Raup D. M and Jablonski D., Springer-Verlag, Heidelberg, Germany, 277–295, dio: 10.1007/978-3-642-70831-2_15, 1986.

445 Sepkoski, J. J., Jr.: Patterns of Phanerozoic extinctions: A perspective from global data bases, in: Global Event Stratigraphy, edited by Walliser, O. H., Springer-Verlag, Berlin, Heidelberg, Germany, 35–52, 1996.

Song, H., Wignall, P. B., Tong, J., and Yin, H.: Two pulses of extinction during the Permian-Triassic crisis., Nat. Geosci., 6, 52–56, doi:10.1038/NGEO1649, 2013.

Song, H., Kemp, D. B., Tian, L., Chu, D., Song, H., and Dai, X.: Thresholds of temperature change for mass extinctions.

450 Nat. Comm., 12, 4694, https://doi.org/10.1038/s41467-021-25019-2 |www.nature.com/naturecommunications, 2021.

Stanley, S. M.: Relation of Phanerozoic stable isotope excursions to climate, bacterial metabolism, and major extinctions, Proc. Nat. Acad. Sci. USA, 107, 19185–19189, www.pnas.org/cgi/doi/10.1073/pnas.1012833107, 2010.

Stanley, S. M.: Estimates of the magnitudes of major marine mass extinctions in earth history, Proc. Nat. Acad. Sci. USA 113, E6325–E6334, www.pnas.org/cgi/doi/10.1073/pnas.1613094113, 2016.

455 Stanley, S. M. and Yang, X.: A double mass extinction at the end of the Paleozoic era, Science, 266, 1340–1344, doi: 10.1126/science.266.5189.1340, 1994.

Svensen, H., Planke, S., Polozov, A. G., Schmidbauer, N., Corfu, F., Podladchikov, Y. Y., and Jamtveit, B.: Siberian gas venting and the end-Permian environmental crisis, Earth Planet. Sci. Lett., 277, 490–500, doi.10.1126/science.1224126, 2009.

460 Timmreck, C., Graf, H-F, Zanchettin, D., Hagemann, S., Kleinen, T., Krüger, K.: Climate response to the Toba super-eruption: Regional changes, Quaternary International, 258, 30-44, doi:10.1016/j.quaint.2011.10.008, 2012.

Vellekoop, J., Sluijs, A., Smit, J., Schouten, S., J. Weijers, W. H., Sinninghe Damsté, J. S., and Brinkhuis H.: Rapid short-term cooling following the Chicxulub impact at the Cretaceous–Paleogene boundary, Proc. Natl. Acad. Sci. USA, 111, 7537–7541, www.pnas.org/cgi/doi/10.1073/pnas.1319253111, 2014.

465 Waters, C. N., Zalasiewicz, J., Summerhayes, C., Barnosky, A. D., Poirier, C., Gałuszka, A., Cearreta, A., Edgeworth, M., Ellis, E. C., Ellis, M., Jeandel, C., Leinfelder, R., McNeill, J. R., deB. Richter, D., Steffen, W., Syvitski, J., Vidas, D., Wagreich, M., Williams, M., Zhisheng, A., Grinevald, J., Odada, E., Oreskes, N., and Wolfe, A. P.: The Anthropocene is functionally and stratigraphically distinct from the Holocene, Science, 351, aad2622, DOI: 10.1126/science.aad2622, 2016.

470 IPCC, 2013: Climate Change 2013: The Physical Science Basis. Contribution of Working Group I to the Fifth Assessment Report of the Intergovernmental Panel on Climate Change, in Stocker, T. F., Qin, D., Plattner, G. K., Tignor, M. M. B.,

Allen, S. K., Boschung, J., Nauels, A., Xia, Y., Bex, V., and Midgley P. M. eds., Cambridge University Press, Cambridge, United Kingdom and New York, USA, pp. 1535, 2013.